Photonic generation of widely tunable phase-coded microwave signals based on a dual-parallel polarization modulator

Shifeng Liu,[1,2] Dan Zhu,[1,2,*] Zhengwu Wei,[1,2] and Shilong Pan[1,2]

[1]*The Key Laboratory of Radar Imaging and Microwave Photonics (Nanjing Univ. Aeronaut. Astronaut.), Ministry of Education, College of Electronic and Information Engineering, Nanjing University of Aeronautics and Astronautics, Nanjing 210016, China*

[2]*State Key Laboratory of Millimeter Waves, Nanjing 210096, China*

**Corresponding author: danzhu@nuaa.edu.cn*

Received March 31, 2014; revised May 22, 2014; accepted May 22, 2014; posted May 27, 2014 (Doc. ID 209213); published June 26, 2014

A photonic approach for the generation of a widely tunable arbitrarily phase-coded microwave signal based on a dual-parallel polarization modulator (DP-PolM) is proposed and demonstrated without using any optical or electrical filter. Two orthogonally polarized ± first-order optical sidebands with suppressed carrier are generated based on the DP-PolM, and their polarization directions are aligned with the two principal axes of the following PolM. Phase coding is implemented at a following PolM driven by an electrical coding signal. The inherent frequency-doubling operation can make the system work at a frequency beyond the operation bandwidth of the DP-PolM and the 90° hybrid. Because no optical or electrical filter is applied, good frequency tunability is realized. An experiment is performed. The generation of phase-coded signals tuning from 10 to 40 GHz with up to 10 Gbit/s coding rates is verified.

OCIS codes: (070.1170) Analog optical signal processing; (050.5080) Phase shift; (060.5625) Radio frequency photonics.

http://dx.doi.org/10.1364/OL.39.003958

In modern radar systems, microwave pulse compression is of great importance to increase the range resolution and detection range [1]. Phase-coded signals with large time-bandwidth product (TBWP) are usually used to perform the pulse compression. The generation of a phase-coded signal in the electrical domain can be realized using either analog or digital electronics, but the operating frequency is usually low and the TBWP is small, limited by the electronic bottleneck. To overcome these problems, the generation of high-frequency and wideband phase-coded signals in the optical domain has been widely investigated thanks to the advantages of high frequency, broad bandwidth, large tunability, and immunity to electromagnetic interference offered by the photonics technologies [2–12]. Phase-coded signal generation based on optical pulse shaping was realized by using a spatial light modulator (SLM) [2]. The advantage of the approach using the SLM is the high flexibility, but the free-space coupling between the optical fiber and the SLM would make the system complicated and lossy. Phase-coded signals can also be generated based on pure fiber-optic schemes. One way is to heterodyne two phase-correlated optical wavelengths with one wavelength phase modulated [3–7], but in practice, it is very difficult to phase modulate one wavelength without affecting the other wavelength since the frequency interval between the two wavelengths is only several to tens of gigahertz. To overcome this problem, various schemes were applied to spatially separate the two wavelengths [4,5] or to map the two wavelengths to two orthogonal polarization directions [6,7]. For these approaches, however, an optical filter or a length of polarization maintaining fiber has to be incorporated, which definitely makes the schemes highly dependent on the optical wavelength or the frequency of the RF signal to be phase coded. Phase coding can also be implemented by a microwave photonic phase shifter based on single sideband polarization modulation [8]. But the single sideband polarization modulation is realized by a polarization modulator (PolM) followed by an optical filter. Again, the frequency range of the system is limited by the optical filter. Recently, a microwave photonic phase-coded RF signal generator without the use of optical filters was proposed based on cascaded PolMs [9], a PolM followed by a PM (phase modulator) [10], a dual-parallel Mach–Zehnder modulator (DPMZM) [11], or a dual-drive Mach–Zehnder modulator (DDMZM) [12]. For these approaches, however, the coding phase has to be fixed at π.

In this Letter, we propose and demonstrate a novel photonic technique to generate widely tunable frequency-doubling arbitrarily phase-coded microwave signals based on a dual-parallel polarization modulator (DP-PolM) [13] without using any optical or electrical filter. An RF signal is fed to the DP-PolM to generate an optical signal with two first-order sidebands having orthogonal polarization states and a suppressed optical carrier. Phase coding is implemented at a following PolM driven by an electrical coding signal. The polarization directions of the two sidebands are aligned with the two principal axes of the PolM. Without any frequency or wavelength dependent components, the scheme can generate frequency-doubling phased-coded signals with ultrawide frequency tuning range. Since the DP-PolM is integratable [13], the scheme can be stable and compact. Frequency tunable phase-coded signal from 10 to 40 GHz being phase coded by up to 10 Gbit/s data sequence is experimentally demonstrated.

Figure 1(a) shows the schematic diagram of the proposed widely tunable frequency-doubling phase-coded

signal generator based on a DP-PolM, which consists of a laser diode (LD), a 90° hybrid, a DP-PolM, a PolM, three polarization controllers (PCs), a polarizer, and a photodetector (PD). A linear polarized light wave from the LD is sent to the DP-PolM via PC1. The two electrical ports of the DP-PolM are driven by two quadrature RF signals by using a 90° hybrid. The DP-PolM is adjusted to produce ± first-order sidebands with carrier suppressed along two orthogonal polarization directions as shown in Fig. 1(b). By adjusting PC2, the two sidebands are coupled into PolM3 with their polarization directions aligned with the two principal axes of PolM3. Because the PolM is a special phase modulator that has opposite modulation indices along the two principal axes, the relative phase of the two sidebands would be controlled by the electrical coding signal introduced to PolM3. The two sidebands are combined by the polarizer and then beat at the PD to generate a frequency-doubling phase-coded signal [6].

As illustrated in Fig. 1(b), the DP-PolM is an integratable modulator consisting of two PolMs, a polarization beam splitter (PBS), a polarization beam combiner (PBC), four PCs, and an optical tunable delay line. For the theoretical analysis, we consider an ideal DP-PolM model with equal performance of the two branches. Similar to [13], the output of the DP-PolM can be expressed as

$$\begin{bmatrix} E_x \\ E_y \end{bmatrix} = E_c e^{j\omega_c t} \begin{bmatrix} \sin\alpha \cdot (e^{j\beta_1\phi_1(t)+j\varphi_1} + e^{-j\beta_1\phi_1(t)}) \\ \cos\alpha \cdot (e^{j\beta_2\phi_2(t)+j\varphi_2} + e^{-j\beta_2\phi_2(t)}) \end{bmatrix}, \quad (1)$$

where E_c and ω_c are the amplitude and the frequency of the optical carrier, α is the angle between the polarization direction of the optical carrier and one of the principal axes of the PBS. β_n is the modulation indices of PolMn($n = 1, 2$), and $\phi_n(t)(n = 1, 2)$ represents the RF signals introduced to PolMn. $\varphi_n(n = 1, 2)$ is a static phase difference between the optical fields along the two principal axes of PolMn at the PBC in the DP-PolM that can be tuned by adjusting the bias voltage of PolMn or by adjusting the PC before the PBC. With the two electrical ports of the DP-PolM being driven by two quadrature RF signals, that is, $\phi_1(t) = \sin(\omega_m t)$ and $\phi_2(t) = \cos(\omega_m t)$, and considering a small signal modulation, we have

$$\begin{bmatrix} E_x \\ E_y \end{bmatrix} = E_c e^{j\omega_c t} \begin{bmatrix} \sin\alpha \cdot (e^{j\beta_1 \sin(\omega_m t)+j\varphi_1} + e^{-j\beta_1 \sin(\omega_m t)}) \\ \cos\alpha \cdot (e^{j\beta_2 \cos(\omega_m t)+j\varphi_2} + e^{-j\beta_2 \cos(\omega_m t)}) \end{bmatrix} = E_c e^{j\omega_c t} \begin{bmatrix} \sin\alpha \cdot [(e^{j\varphi_1} - 1) \cdot J_{-1}(\beta_1) \cdot e^{-j\omega_m t} + \ldots \\ (e^{j\varphi_1} + 1) \cdot J_0(\beta_1) + (e^{j\varphi_1} - 1) \cdot J_1(\beta_1) \cdot e^{j\omega_m t}] \\ \cos\alpha \cdot [j(1 - e^{j\varphi_1}) \cdot J_{-1}(\beta_2) \cdot e^{-j\omega_m t} + \ldots \\ (e^{j\varphi_1} + 1) \cdot J_0(\beta_2) + j(e^{j\varphi_1} - 1) \cdot J_1(\beta_2) \cdot e^{j\omega_m t}] \end{bmatrix}, \quad (2)$$

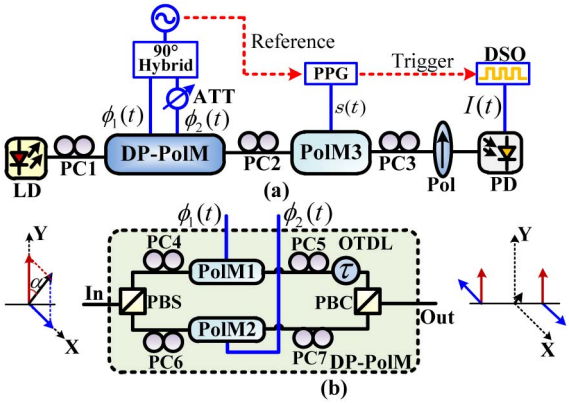

Fig. 1. (a) Schematic diagram of the proposed phase-coded signal generator based on a DP-PolM. LD, laser diode; PC, polarization controller; DP-PolM, dual-parallel polarization modulator; ATT, electrical attenuator; PolM, polarization modulator; Pol, polarizer; PD, photodetector; PPG, pulse pattern generator; DSO, digital sampling oscilloscope. (b) Illustration of the DP-PolM. OTDL, optical tunable delay line; PBS, polarization beam splitter; PBC, polarization beam combiner.

where J_n is the nth-order Bessel function of the first kind. By tuning PC5 and PC7 to make $\varphi_1 = \varphi_2 = \pi$, the optical carrier will be suppressed at the output of DP-PolM. β_1 and β_2 are made to be equal by adjusting the electrical attenuator. α is tuned to be $\pi/4$. Then we get

$$\begin{bmatrix} E_x \\ E_y \end{bmatrix} = \sqrt{2} E_c \cdot J_1(\beta) \cdot e^{j\omega_c t} \begin{bmatrix} e^{-j\omega_m t} - e^{j\omega_m t} \\ -j \cdot e^{-j\omega_m t} - j \cdot e^{j\omega_m t} \end{bmatrix}. \quad (3)$$

As can be seen from Eq. (3), with equal amplitude and orthogonal polarization states, the ± first-order sidebands of E_x are out of phase while the ± first-order sidebands of E_y are in phase, as shown in Fig. 1(b). The transfer function of PC2 can be written as [14]

$$P_F = \begin{bmatrix} \cos\theta_1 & -\sin\theta_1 \\ \sin\theta_1 & \cos\theta_1 \end{bmatrix} \begin{bmatrix} e^{j\delta_1} & 0 \\ 0 & e^{-j\delta_1} \end{bmatrix}, \quad (4)$$

where θ_1 is the rotator angler, and δ_1 is the phase difference between E_x and E_y introduced by PC2. After passing through PC2, the optical field is

$$\begin{bmatrix} E_{x\text{-pc2}} \\ E_{y\text{-pc2}} \end{bmatrix} = \begin{bmatrix} \cos\theta_1 & -\sin\theta_1 \\ \sin\theta_1 & \cos\theta_1 \end{bmatrix} \begin{bmatrix} e^{j\delta_1} & 0 \\ 0 & e^{-j\delta_1} \end{bmatrix} \begin{bmatrix} E_x \\ E_y \end{bmatrix} = \begin{bmatrix} E_x \cdot e^{j\delta_1} \cdot \cos\theta_1 - E_y \cdot e^{-j\delta_1} \cdot \sin\theta_1 \\ E_x \cdot e^{j\delta_1} \cdot \sin\theta_1 + E_y \cdot e^{-j\delta_1} \cdot \cos\theta_1 \end{bmatrix}. \quad (5)$$

By setting PC2 to make θ_1 to be $\pi/4$ and δ_1 to be $-\pi/4$, we have

$$\begin{bmatrix} E_{x\text{-pc2}} \\ E_{y\text{-pc2}} \end{bmatrix} = 2E_c J_1(\beta) \cdot e^{j\omega_c t - j\pi/4} \begin{bmatrix} -e^{j\omega_m t} \\ e^{-j\omega_m t} \end{bmatrix}. \quad (6)$$

As can be seen, the polarization states of the two first-order sidebands are orthogonal. When the two optical sidebands are coupled to PolM3, they are phase modulated with opposite phase shifts [6]. The output of the polarizer following PolM3 and PC3 is

$$E_{\text{out}} = \sqrt{2}E_c J_1(\beta) e^{j\omega_c t - j\pi/4}(-e^{j\omega_m t + j\pi V_s s(t)/V_\pi + j\varphi_3} + e^{-j\omega_m t - j\pi V_s s(t)/V_\pi}), \quad (7)$$

where V_π is the half-wave voltage of PolM3, $s(t)$ is the applied phase encoding signal with amplitude of V_s, and φ_3 is the phase difference between the orthogonal components introduced by DC bias of PolM3 or PC3. In the derivation, φ_3 is set to be π by adjusting PC3. Applying E_{out} to a PD with responsivity of $\Re$ for square-law detection, the generated electrical signal is

$$I(t) \propto \Re E_{\text{out}} \cdot E_{\text{out}}^* \propto 4\Re E_c^2 \cdot J_1(\beta)^2 \cos[2\omega_m t + 2\pi V_s s(t)/V_\pi]. \quad (8)$$

As can be seen from Eq. (8), a frequency-doubling signal phase coded by $s(t)$ is generated.

An experiment based on the setup shown in Fig. 1 is carried out. Since the integrated DP-PolM is not available, an equivalent setup using two PBSs, four PCs, and two PolMs with a bandwidth of 40 GHz is used in our experiment. The key limitation of the use of discrete components is the inequality between the two branches and the instability introduced by the environment. An electrical attenuator is used to properly adjust the RF power applied to the two branches according to the half-wave of corresponding PolM to realize the equality of the two branches. A tunable optical delay line is incorporated to ensure that the two signal paths are identical. Once the DP-PolM is integrated, the inequality will be eliminated. The parameters of the other key devices are as follows: the LD has a linewidth of 2.1 kHz and an output power of 19 dBm (Teraxion NLL04). PolM3 (Versawave Technologies) has a bandwidth of 40 GHz and a half-wave voltage of 3.5 V. The PD (u^2t Photonics, XPDV2150R) has a bandwidth of 50 GHz and a responsivity of 0.65 A/W. The electrical coding signal is generated by a pulse pattern generator (Anritsu MP1763C), and the RF signals are generated by an analog signal generator (Agilent 8267D). An optical spectrum analyzer (Yokogawa AQ6370C) with a resolution of 0.02 nm is employed to monitor the optical spectra. And a 40 GHz digital sampling oscilloscope (Agilent 86100A) is used to observe the waveforms.

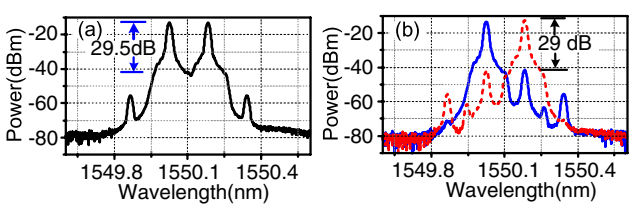

Fig. 2. Optical spectra (a) of the signal at the output of the DP-PolM and (b) the orthogonally polarized signals split by a PBS connected to PC2.

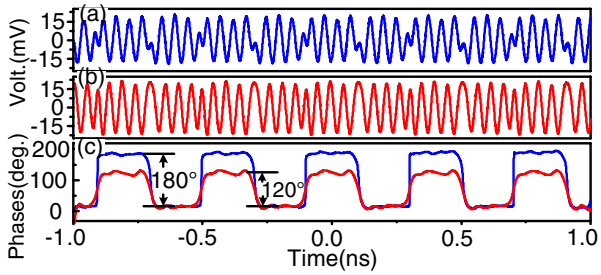

Fig. 3. 20 GHz phase-coded waveforms with the coding signal's amplitude voltage set to (a) 1.77 V, and (b) 1.20 V; (c) respective recovered phase-coding signals corresponding to (a) (blue solid) and (b) (red solid).

With the DP-PolM driven by two quadrature 10 GHz RF signals, Fig. 2 shows the optical spectra at the output of the DP-PolM. As can be seen in Fig. 2(a), the optical carrier is effectively suppressed, and the ± first-order sidebands are 29.5 dB higher than the carrier. To verify that the two sidebands are along two orthogonal polarization axes, a PBS is connected to the output of PC2 following the DP-PolM. Figure 2(b) shows the optical spectra of the two orthogonally polarized signals at the two output ports of the PBS. As can be seen, the two sidebands are indeed orthogonal. When a 5 Gbit/s encoding signal with a pattern of "0101" is applied to the PolM3, Figs. 3(a) and 3(b) show the waveforms of the 20 GHz frequency-doubling phase-coded signals. The voltage amplitude of the encoding signal $s(t)$ is set to be 1.77 V and 1.20 V. As the half-wave voltage of PolM3 is about 3.5 V, the theoretically calculated phase shifts corresponding to bit "1" are 180° and 120°, respectively, for each case. Figure 3(c) shows the recovered phase-coded signals corresponding to Figs. 3(a) and 3(b). As can be seen, the 20 GHz frequency-doubling signal is successfully arbitrarily phase coded, and the experimental results are consistent with the theoretical prediction. The PolM is a traveling-wave modulator that is designed to match the velocities of the light wave and the microwave signal, thus the temporal drift of each branch is relatively weak [15].

The pulse-compression capability is also investigated. By applying a 5 Gbit/s 16 bit encoding signal of "1111 0110 1001 1010" with amplitude of 1.77 V, the waveform of the generated phase-coded signal and the

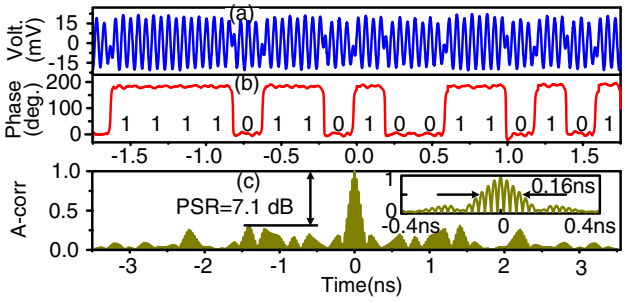

Fig. 4. (a) Waveforms of the 5 Gbit/s phase-coded 20 GHz signal; (b) the recovered phase profile; (c) autocorrelations of the generated signal. Inset of (c): zoom-in views of the peak.

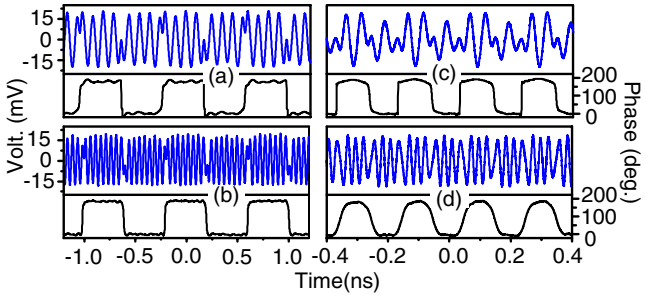

Fig. 5. Waveforms (blue solid) of the 2.5 Gbit/s phase-coded signals with (a) 10 GHz (b) 20 GHz RF carrier; and the 10 Gbit/s phase-coded signals with (c) 20 GHz (d) 40 GHz RF carrier; and the corresponding recovered phases (black solid).

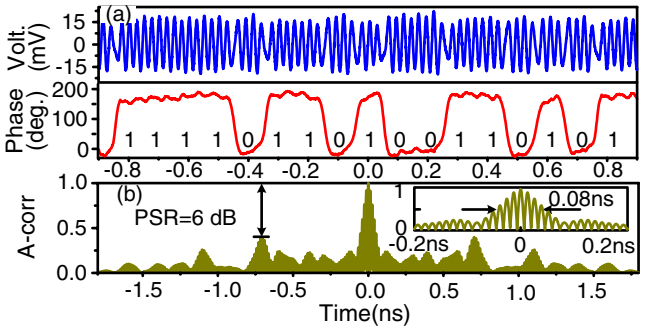

Fig. 6. (a) Waveform of the 10 Gbit/s phase-coded 40 GHz microwave signal and the recovered phase profile. (b) Autocorrelations of the measured signal. Inset of (b): zoom-in views of the peak.

corresponding recovered phase are shown in Figs. 4(a) and 4(b), respectively, with time duration of 3.5 ns. The compressed result of the signal through autocorrelation is shown in Fig. 4(c). As can be seen, the full width at half-maximum (FWHM) of the peak pulse is about 0.16 ns, corresponding to a compression ratio of about 20. The peak-to-sidelobe ratio (PSR) is about 7.1 dB, which is comparable to those of [4,11], and [12].

Good frequency tunability can be realized because no optical or electrical filter is applied. The only limitation is the bandwidth of the PolM and the PD. To demonstrate the frequency tunability of the proposed scheme, the RF signal applied to the DP-PolM is tuned from 5 to 20 GHz. Waveforms of the 2.5 Gbit/s phase-coded signals with 10 and 20 GHz frequency-doubling carrier and the corresponding recovered phases are shown in Figs. 5(a) and 5(b), respectively, with time duration of 2.4 ns. Increasing the coding rate to 10 Gbit/s, the waveforms of the generated signals with time duration of 0.8 ns and the recovered phases with 20 GHz and 40 GHz RF carrier are shown in Figs. 5(c) and 5(d), respectively. The voltage amplitude of the encoding signal is 1.77 V in all cases. Again, π-shift phase-coded signals are successfully generated with widely tunable frequency range and different coding rates. To investigate the pulse-compression capability, a 10 Gbit/s 16 bit coding signal with the pattern of "1111 0110 1001 1010" is applied. Figure 6(a) shows the waveform of the signal and the recovered phase with time duration of 1.8 ns. The autocorrelation result in Fig. 6(b) shows that the FWHM of the peak pulses is 0.08 ns and the PSR is about 6.0 dB. A compression ratio of 20 is achieved. The compression ratio is not as large as that in [4] and [7], which is mainly due to the lower data rate and shorter code length used in the experiment.

In conclusion, we propose and demonstrate a photonic approach for the generation of a widely tunable phase-coded signal based on a DP-PolM. Because no optical or electrical filter is applied, good frequency tunability is realized. The inherent frequency-doubling operation can make the system work at a frequency beyond the operation bandwidth of the DP-PolM and the 90° hybrid. Phase-coded signals with frequencies tuning from 10 GHz to 40 GHz and coding rates up to 10 Gbit/s are experimentally generated. The working bandwidth can be improved by improving the working bandwidth of the PD. This approach has potential applications in frequency-agile radar systems.

This work was supported in part by the National Basic Research Program of China (2012CB31575), the National Natural Science Foundation of China (61201048, 61107063), the Natural Science Foundation of Jiangsu Province (BK2012381, BK2012031), the Aviation Science Foundation of China (2013ZC52040, 2012ZD52052), the Postdoctoral Science Foundation of China (2013T60533, 2012M521078), the Jiangsu Planned Projects for Postdoctoral Research Funds (1102054C), and the Foundation of Graduate Innovation Center in Nanjing University of Aeronautics and Astronautics (kfjj130113).

References

1. M. I. Skolnic, *Introduction to Radar* (McGraw-Hill, 1962).
2. J. Chou, Y. Han, and B. Jalali, IEEE Photon. Technol. Lett. **15**, 581 (2003).
3. P. Ghelfi, F. Scotti, F. Laghezza, and A. Bogoni, J. Lightwave Technol. **30**, 1638 (2012).
4. Z. Li, W. Z. Li, H. Chi, X. M. Zhang, and J. P. Yao, IEEE Photon. Technol. Lett. **23**, 712 (2011).
5. H. Y. Jiang, L. S. Yan, J. Ye, W. Pan, B. Luo, and X. Zou, Opt. Lett. **38**, 1361 (2013).
6. H. Chi and J. Yao, IEEE Microw. Wirel. Compon. Lett. **18**, 371 (2008).
7. Z. Li, M. Li, H. Chi, X. M. Zhang, and J. P. Yao, IEEE Microw. Wirel. Compon. Lett. **21**, 694 (2011).
8. Y. M. Zhang and S. L. Pan, Opt. Lett. **38**, 766 (2013).
9. L. Gao, X. F. Chen, and J. P. Yao, IEEE Photon. Technol. Lett. **25**, 899 (2013).
10. W. Li, L. X. Wang, M. Li, and N. H. Zhu, Opt. Lett. **38**, 3441 (2013).
11. W. Li, L. X. Wang, M. Li, H. Wang, and N. H. Zhu, IEEE Photon. J. **5**, 5501507 (2013).
12. Z. Z. Tang, T. T. Zhang, F. Z. Zhang, and S. L. Pan, Opt. Lett. **38**, 5365 (2013).
13. M. H. Huang, J. B. Fu, and S. L. Pan, Opt. Lett. **37**, 1823 (2012).
14. W. L. Liu, M. G. Wang, and J. P. Yao, J. Lightwave Technol. **31**, 1636 (2013).
15. J. D. Bull, N. A. Jaeger, H. Kato, M. Fairburn, A. Reid, and P. Ghanipour, Proc. SPIE **5577**, 133 (2004).